Porous hydroxyapatite-based obturation materials for dentistry

Witold Brostow[a)]
Laboratory of Advanced Polymers & Optimized Materials, Department of Materials Science and Engineering, University of North Texas, Denton, Texas 76203-5310

Miriam Estevez
Centro de Física Aplicada y Tecnología Avanzada, Universidad Nacional Autónoma de México, Querétaro, Qro. 76000, México

Haley E. Hagg Lobland and Ly Hoang
Laboratory of Advanced Polymers & Optimized Materials, Department of Materials Science and Engineering, University of North Texas, Denton, Texas 76203-5310

J. Rogelio Rodriguez
Centro de Física Aplicada y Tecnología Avanzada, Universidad Nacional Autónoma de México, Querétaro, Qro. 76000, México; and Centro de Investigación y Estudios Avanzados del Instituto Politécnico Nacional, Querétaro, Apdo. Postal 1-798, Qro., 76001, México

Susana Vargar
Centro de Física Aplicada y Tecnología Avanzada, Universidad Nacional Autónoma de México, Querétaro, Qro. 76000, México

(Received 28 August 2007; accepted 4 January 2008)

New porous biomaterials based on hydroxyapatite (HAp) were designed as obturation materials for dental cavities. Synthetic HAp powder with a particle diameter of 150 μm was agglutinated using three different polyurethane monocomponents (rigid, semi-rigid, and flexible), enabling the matching of their properties to those of real teeth. Alumina particles were also added in some cases. Our new hybrid materials contain up to 60% HAp. Interconnected pores range in size from 100 to 350 μm, while the pore volume fraction varies between 25% and 60%. Most of these materials possess the right morphology for implants and prostheses because their porous structures can be vascularized for bone and tooth ingrowth. Some samples also contain alumina particles to improve the abrasion resistance and to support the stresses produced during mastication. The materials were characterized by x-ray diffraction, scanning electron microscopy, and mechanical testing, along with abrasion, scratch, sliding wear, friction, and staining tests.

I. INTRODUCTION

Numerous different types of biomaterials have been designed for human implants or prostheses, specifically for bone repair or bone ingrowth (e.g., traumatism and bone disease). However considerably less effort has been addressed to implants capable of tooth ingrowth.[1–3] For tooth and bone implants, a primary requirement is that the material be bioaccepted, because vascularization requires the material to support cellular activity without eliciting an inappropriate host response on recognition of the foreign molecules (i.e., molecular recognition).[4] Second, the morphology must be suitable to allow vascularization and attachment to the existing bone or tooth substrates.[5,6]

Morphological specifications for bone-implant materials require a pore size in the range of 100–400 μm, with the pores being interconnected and comprising a volume fraction between 50% and 70%.[7] For tooth implants, on the other hand, the mean optimal pore size is 2.90 ± 0.22 μm (standard deviation), which is considerably smaller.[8] A precise densitometry study[9] showed that enamel has a density distribution that is narrower with respect to that of dentin: namely, the density of enamel is reportedly between 2.49 and 3.00 g/mL (mean density 2.94 ± 0.03 g/mL), while the density of dentin is between 2.06 and 2.24 g/mL (mean density 2.14 ± 0.01 g/mL). Using these values, it is possible to demonstrate that the pore volume fraction of dentin is around 27%, a value in good agreement with that of 22%, which was obtained

a)Address all correspondence to this author.
e-mail: brostow@unt.edu
DOI: 10.1557/JMR.2008.0191

using results that have been reported elsewhere.[8] One observes then that pore size and pore volume fraction are smaller for dentin than for bone.[7–12]

While porous materials have many important applications in, for example, acoustic and thermal insulation, transportation, filtration, purification, biomaterials, building constructions,[13] a new generation of porous biomaterials has recently emerged enabling one to better reproduce the structure of natural bone. Several groups[14,15] have been successful in controlling the size, volume, and interconnectivity of pores in their materials. Nevertheless, there have been only a few reports[16–18] on the use of porous materials for dental fillings: a possible reason for this is that porous materials tend to have poor mechanical properties, while the mastication process produces high compression and shear stresses that must be supported by the obturation material. Consequently, nonporous materials, usually hard polymer resins, are more commonly used to support these stresses. However, we claim in this article that, by the selection of an appropriate agglutinating polymer (for a ceramic filler), it is possible to create porous materials with suitable morphology and mechanical strength.

Beyond achieving the correct morphology, a successful dental obturation material must be chemically compatible with and adhere to the substrate.[19–23] Many obturation materials are designed essentially by controlling only mechanical properties because adding a ceramic, or generally a filler, is known to improve the mechanical properties of polymers.[24] Here, we take into account morphology, chemical structure, mechanical behavior, and surface properties, considering the combined effect of all of these on tooth ingrowth,[25–27] as well as the role of viscoelasticity for implant compliance and performance.[28,29]

Because teeth constitute an organic–inorganic hybrid, a reliable hybrid[30] for dental applications[31] should contain an agglutinating polymer that possesses: (i) high shear strength (around 70 MPa) resistance interfacial stresses during mastication; (ii) appropriate tensile/compressive strength and toughness, because very rigid and tough materials may lead to premature wear of the real teeth from contact during chewing[32]; (iii) high scratch resistance, to avoid the occurrence of fissures, cracks, or canals that invite bacterial growth; (iv) good adhesion with the hydroxyapatite (HAp) powder particles and with the substrate (dentin) to avoid microfiltration, which produces bacterial growth[29,32,33]; (v) high hydrolytic stability[34–36] for durability within the environmental conditions of the mouth; and (vi) appropriate chemistry, to favor nonaggravating molecular recognition by the immune system. For all composites of the general type polymer plus ceramic, the problem of adhesion between differing components is an important challenge in product development.[37–40] In turn, adhesion depends on surface and interfacial tension values.[41]

Based on these specifications, we selected a polyurethane (PU) monocomponent, cross-linkable at room temperature, as the agglutinating polymer for our HAp-based hybrids. PUs have a large variety of structures and thus a variety of properties, from flexible to rigid.[42,43] Our polyisocyanate cross-linker contains a blocking functionality that limits its own chemical reactivity, thereby stabilizing the resin-plus-isocyanate mixture. In the presence of moisture, part of the blocking structure is released, producing, in this particular case, CO_2, while the rest reacts with –OH groups that are present in the material (e.g., on HAp, the hydroxylated PU resin). The result of the reaction between the HAp and the polymeric resin is the production of a network in which HAp particles act as hubs, with polymer molecules chemically anchored to their surface and joining different HAp particles through polymer bridges.[44] This network morphology of our chemically reacted hybrid improves the mechanical properties compared to physical blends of the same type of material.

Furthermore, the CO_2 produced during the chemical reaction that occurs when the resin and cross-linker are mixed with HAp particles acts as a pore-former, creating a porous material. Both pore size and pore volume fraction in the material depend on (i) the HAp particle size (and the surface area of HAp particles that is exposed when the chemical reactions take place) and (ii) the relative proportion of polyisocyanate (i.e., the –OH groups in the reactive mixture).

Here we describe the synthesis of new porous HAp-based materials that can be produced in situ at room temperature and without the presence of other undesirable compounds such as pore-formers or other reaction sideproducts. At the same time, our process is designed so that we can control the morphology while also achieving good adhesive, mechanical, and wear properties.

II. EXPERIMENTAL

A. Synthesis

A rigid PU resin was prepared from a commercially available aliphatic (acrylic) hydroxylated resin (Reichhold, Research Triangle Park, NC) combined with a malonate-blocked polyisocyanate (prepared in the laboratory) as the curing agent (CA) in a proportion of 4:1 by volume (to react all cyano groups). Using the same resin/CA ratio and the same CA, a flexible PU resin was prepared from a commercial aromatic hydroxylated resin (Bayer, Leverkusen, Germany) while a semi-rigid sample was obtained by mixing equal proportions of the rigid and flexible resins. The reactions occurred at room temperature, and chemical compositions of the samples are reported in Table I.

TABLE I. Chemical composition and physical properties of the prepared samples.

Samples	HAp (g)	PU resin (g)	Alumina (g)	Density of solid material (g/cm^{-3})	Density of porous material (g/cm^{-3})	Stain penetration (mm)
R-100	6.0	5.0	0.0	1.547	0.762	0.46
R-100-201	4.8	5.0	1.2	1.528	0.627	0.00
R-100-40	3.6	5.0	2.4	1.541	0.817	0.00
SR-100	6.5	5.0	0.0	1.545	1.004	0.40
F-100	7.0	5.0	0.0	1.542	1.141	0.22

B. Sample preparation

Small disks of 1 cm diameter and 0.5 cm thickness were produced at room temperature by mixing synthetic HAp [$Ca_{10}(PO_4)_6(OH)_2$] powder (Sigma Aldrich, Milwaukee, WI) ground at a mesh of 100 (particles 150 μm diameter) with the three different PU monocomponent resins: rigid; semi-rigid; and flexible. Once a homogeneous paste was obtained, the mixture was placed in Teflon (DuPont, Wilmington, DE) molds to produce the disks. Samples were kept in the molds for 24 h to ensure full curing of the thermoset resins. For some samples, alumina microparticles (1.4 μm diameter) were added (at 20 and 40 wt% with respect to HAp).

C. Staining

By rubbing recently prepared samples with a spatula or other flat object, the pores of the surface are closed, leaving a smooth (poreless) surface. Some of the samples were rubbed until smooth and then soaked for 2 weeks in an aqueous solution of methylene blue (MB), a common staining agent. After that time, the samples were removed from the staining liquid and cut down the middle. The MB penetration was measured from the cross section using an optical microscope. The results of the microfiltration test are reported in Table I.

D. X-ray diffraction

The x-ray diffraction (XRD) patterns were obtained using a Rigaku (Tokyo, Japan) D500 machine with a radiation source of 0.154 nm. The angle 2θ was varied from 10° to 80° at a rate of 2°/min.

E. Density

The densities were determined by weighing the samples on an analytical balance (resolution 1×10^{-5} g) and measuring the disk sizes with a micrometer (resolution 1×10^{-4} cm).

F. Scanning electron microscopy

Scanning electron microscopy (SEM) was performed with a JEOL (Tokyo, Japan) JSM-6060 scanning electron microscope at 20 kV in secondary electron mode with different magnifications. Samples were frozen in liquid N_2 and broken, and the new fractured surface was coated with gold. Average pore sizes were determined from SEM images by measuring the diameters of >200 pores for each sample.

G. Tensile mechanical tests

Mechanical tests were performed in an Adamel Lhomargy (Konkonkoma, NY) machine model DY.22 at 2.5 cm/min. The experiments were performed (five times for each sample type) in a three-point-bending configuration with two supports separated by 2.0 cm and the pressure applied in the middle by the probe.

H. Abrasion testing

Abrasion experiments were performed on a specially designed apparatus using the Taber method according to the ASTM-D-1242-95 standard, using a steel disk of 25.5 cm radius rotating at 250 revolutions per minute (rpm) with sandpaper Fandeli (Houston, TX) F-120 adhered on its surface. Samples were placed on the rotating disk, and a load of 10 g was applied; every 20 s, the weight loss was determined using an analytical balance (resolution 1×10^{-5} g). After the sanding process and before the weight determination, the sanded surface was wiped clean with a dry, soft cloth while the sandpaper was cleaned with a soft brush to remove dust. All experiments were performed at room temperature under dry conditions for a total time of 200 s. Five sets of abrasion experiments were performed for each sample.

I. Scratch resistance

Scratch resistance was determined on a microscratch tester (CSEM Instruments, Neuchatel, Switzerland) equipped with a Rockwell diamond tip (radius 200 mm, included angle 120°). The procedure has been described before.[45–49] During single scratch tests, the instantaneous penetration depth R_p was recorded over the length of 5-mm-long scratch grooves. Scratching was conducted at 5 mm/min under applied loads between 5 N and 25 N. The residual depth R_h of the scratch groove was recorded afterward under an applied load of 0.03 N to measure the amount of viscoelastic recovery (f). The percentage f was quantified according the following equation, which was first defined in Ref. 45 (see also Ref. 46):

$$f = \left(1 - \frac{R_h}{R_p}\right) \times 100\% \quad . \tag{1}$$

The reported values of R_p and R_h are averages of the values obtained between 0.5 and 4.5 mm along the scratch groove.

J. Sliding wear

As with the single scratch tests defined immediately above, sliding wear tests were conducted using the same

microscratch tester, similarly equipped, and at the same sliding speed of 5 mm/min. The principles of sliding wear determination and the resulting (in most cases) strain hardening have been described before.[50–52] The test consists of multiple (usually $\geqslant$15) consecutive scratches across the same groove during which the R_p and R_h are recorded for each pass. Such repetitive passes of the indenter simulate the wear that occurs in real applications. As with tests of scratch resistance, the values reported are averages of values obtained along the 5-mm-long scratch groove between 0.5 and 4.5 mm. We recall that the percentage f defined by Eq. (1) that was obtained from sliding wear tests has been related to brittleness B, which was defined in Ref. 52. The resulting exponential relation between B and f has been found valid for all polymers despite vast differences in their properties.

K. Friction

Friction was evaluated using a Nanovea pin-on-disk tribometer (Microphotonics, Irvine, CA) equipped with a silicon nitride pin. Samples were tested under an applied force of 2 N during 5000 revolutions at 100 rpm.

III. CHEMICAL AND PHYSICAL CHARACTERIZATION

A. Structural stability

The XRD patterns of HAp-plus-resin and HAp-plus-resin-plus-alumina hybrids were compared to the patterns for pure HAp and alumina. The patterns show that the chemical reaction between the HAp and the isocyanate does not modify the crystalline structure of HAp or the alumina. All of the characteristic reflections of HAp and alumina appear in the hybrid material, indicating unaltered crystalline structures.

Because our purpose was to use the hybrids as obturation materials, the hydrolytic stability and morphology of the samples are important properties to define. The sample names are preceded by R (rigid), SR (semi-rigid), and F (flexible), with compositions as defined in Table I. We have determined that when pore size is >2.9 μm and porosity is around 27% by volume, the whole system is percolated with an interconnected structure of pores that potentially can be appropriate for vascularization and therefore for the regeneration of teeth.

B. Morphology of porous samples

The rigid, semi-rigid, and flexible hybrids all possess a porous morphology. We see in the R-100 sample in Fig. 1(a) large interconnected pores in the range from 90 to 350 μm (mean size 138 ± 76 μm, Fig. 2). We note that a Serbian group has reported[53] a minimum pore size of 0.4 μm. The effects of pore size on mechanical properties will be discussed in Sec. IV. B. We found similar results in Fig. 1(c) for the rigid sample containing 20% alumina (R-100-20). The pore size of R-100-20 ranges from 150 to 370 μm, but the mean size is 249 ± 98 μm. In addition to the large interconnected pores, there are many small closed pores (<50 μm) that may reduce the

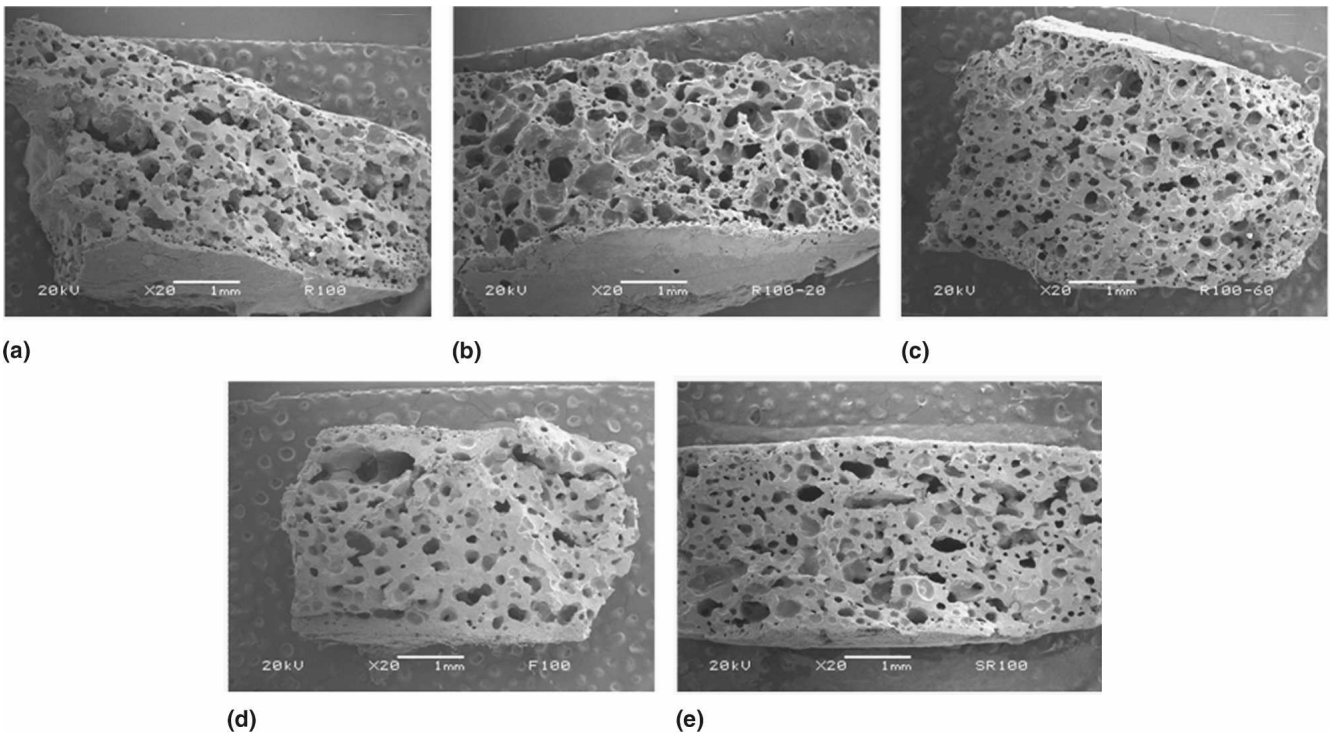

(a) (b) (c)

(d) (e)

FIG. 1. SEM micrographs of all samples at 20×: (a) R-100; (b) R-100-20; (c) R-100-40; (d) F-100; and (e) SR-100.

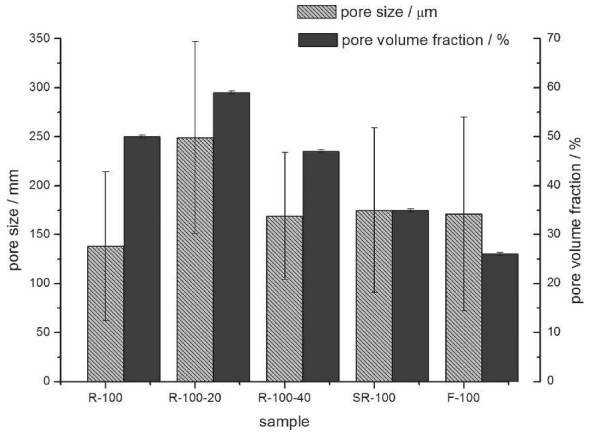

FIG. 2. Values of the pore size and pore volume fraction for all samples.

mechanical properties and are not suitable for vascularization. Sample R-100-40 in Fig. 1(c) appears similar to the R-100 sample, with large pores between 100 and 300 μm and a mean size of 169 ± 65 μm. Figure 1(c) also indicates that the R-100-40 sample contains fewer small closed pores than the R-100-20 sample.

By contrast, we found small pores in the sample seen in Fig. 1(d) that were uniformly distributed along the entire sample with just a few large interconnected pores for the flexible material F-100. The pores in the F-100 material range in size from 100 to > 400 μm with a mean size of 171 ± 99 μm. Thus, the average pore size reflects the abundance of small pores combined with only a few larger ones. Not surprisingly, the morphology of the semi-rigid sample SR-100 reflects its flexible and rigid components. In Fig. 1(e), large interconnected pores are clearly visible; their sizes range from 100 to > 300 μm, with a mean size of 175 ± 84 μm. Although this numerical average is similar to that for the R-100-40 sample, we observe that the SR-100 sample has significantly more closed (blind) pores that do not contribute to the vascularization.

C. Density and volume fraction of pores

As stated earlier, it is known that the pore volume fraction must be about 27% to percolate the system. The volume fraction of pores ϕ_p in the prepared samples was calculated from the densities of a solid nonporous (ρ_s) sample and a porous (ρ_p) sample of the same composition according to the relationship:

$$\phi_p = 1 - \frac{\rho_p}{\rho_s} \quad . \qquad (2)$$

Nonporous samples were prepared in the same way as described above for porous samples but using an isocyanate without the blocking group, thereby eliminating the formation of CO_2. The densities listed in Table I were calculated from the mass, as measured on an analytical balance, divided by the volume (determined by measuring the sample size on a micrometer).

The pore volume fractions calculated from Eq. (1) are also reported in Fig. 2 (along with pore size). We found that the mean pore volume fraction was smallest (26 ± 0.3%) for the F-100 sample. The remaining samples have higher ϕ_p values that lie between 35% and 59%, all of which are suitable in terms of their potential for allowing vascularization.

D. Stain susceptibility

The microfiltration of the MB stain does not appear to directly correlate with either pore size or pore volume. The data in Table I indicate that stain penetration was immeasurable for the rigid samples containing alumina and <0.5 mm for the other sample compositions.

IV. MECHANICAL AND TRIBOLOGICAL CHARACTERIZATION

A. Abrasion

Because the mastication process imposes significant shear stresses that scratch and abrade the teeth, it is essential to obtain a filling material with sufficient durability. The results of our abrasion experiments are reported in Fig. 3(a), where weight loss is plotted as a function of abrasion time (up to 200 s for all samples). The dependence of weight loss on abrasion time is nearly linear, with the slopes of the lines corresponding to the time rate of weight loss [values in Fig. 3(b)]. The semi-rigid sample SR-100 performed the worst, losing weight at a rate of 0.063 mg/s (or 3.78 mg/min). With a weight loss rate of 0.055 mg/s, the R-100 sample performed somewhat better. The addition of alumina provides an improvement: Fig. 3(b) shows rates of 0.046 mg/s and 0.047 mg/s, respectively, for the R-100-20 and R-100-40 samples. These two samples have practically the same abrasion resistance despite a difference in pore size and pore volume fraction. Apparently, doubling the alumina concentration has a negligible effect. [The errors for the rates of weight loss are provided in Fig. 3(b).]

The sample with the highest abrasion resistance was the F-100 sample, which lost weight at 0.032 mg/s: this value is practically half that of the semi-rigid sample. In this scenario, a flexible resin is beneficial because softer materials are more difficult to grind and generate less particulate debris. Furthermore, the presence of several large pores with diameters >300 μm may contribute to the poor abrasion resistance of the SR-100 sample. Moreover, as the subsequent section on mechanical properties suggests, the rigid component of the SR-100 sample seems to have more influence on the sample properties than does the flexible component (at the concentration used).

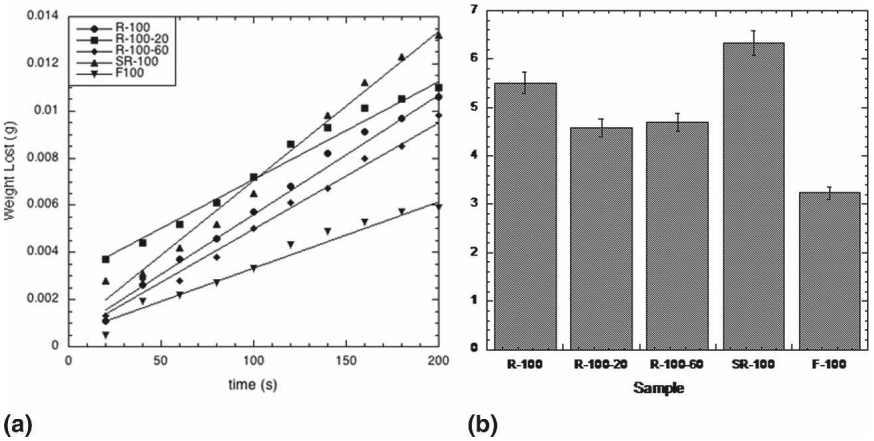

FIG. 3. Abrasion results: (a) weight loss versus abrasion time and (b) weight loss rate for all samples. Standard deviation is reported for n = 5.

B. Mechanical properties

We report the outcome of mechanical tests in Fig. 4. For all samples, the Young's modulus is fairly low as a result of porosity in the materials. This is a widespread effect in porous materials compared to their nonporous counterparts. The pores create many points for stress concentration, while their thin walls favor crack propagation and fissures as a result of the high local stresses. We recall molecular-dynamics computer simulations of polymeric materials: small cracks can grow into large ones (unless crack arrest occurs).[54,55] However, some investigators[56] have demonstrated that the Young's modulus can be increased significantly when an organic phase (e.g., collagen) fills the interconnected pores. Here also, we see the clear effects of pores and of the composition variation. The F-100 sample has the lowest modulus by far for two reasons: it has the lowest ϕ_p; and the flexibility of the PU.

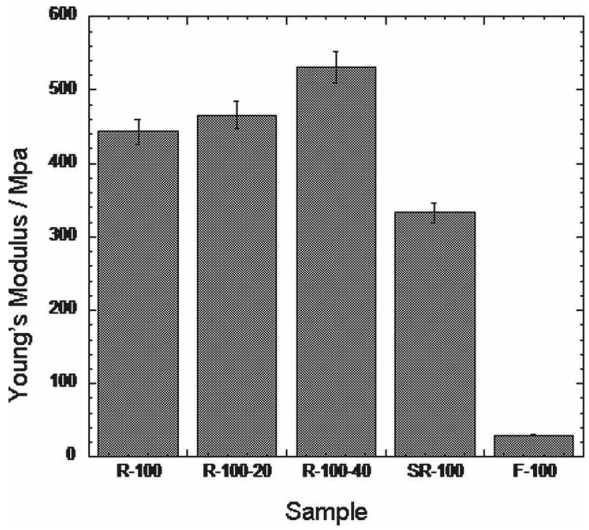

FIG. 4. Young's modulus for all samples. Standard deviation is reported for n = 5.

As expected based on our previous work,[29,45] tough ceramic particles improve the mechanics as well as the tribology of the hybrid materials, as manifested in the moduli and also in the improved abrasion resistance. Thus, the two samples with Al_2O_3 are the strongest. The R-100-40 sample, which has the most alumina, has the highest modulus of all; both the R-100-20 and R-100-40 samples contain the same amount of PU. Quite pertinent also is the result for the R-100 sample; its modulus is only slightly lower than that of the R-100-20 sample. This means that the reinforcement effect caused by a rigid PU filling large pores is much larger than that caused by the presence of Al_2O_3. However, return now to Fig. 3(b). The alumina-containing samples have lower abrasion rates than the other samples, except for the F-100 sample, which has small pores and a flexible PU. Thus, if optimization with respect to both modulus and abrasion resistance is needed, the R-100-20 sample would be the material of choice.

C. Scratch resistance and sliding wear

We see in Fig. 5 the penetration R_p and residual depth R_h values corresponding to single scratch tests at forces between 5 N and 25 N. For all samples, both R_p and R_h increase with increasing load, as expected. While the responses of some types of materials are linear, the wavy nature of the R_p and R_h curves for other materials is due to porosity and the particulate nature of our materials. For instance, the maxima observed for the F-100 and SR-100 samples can come from hitting a thin-walled pore, where the diamond indenter is able to penetrate more deeply. Furthermore, we observe that, overall, the R_p is the highest in the flexible material while the R_h is simultaneously the most shallow. A softer material is more easily penetrated but experiences greater viscoelastic recovery *f*. The rigid sample R-100 has the smallest R_p and also better *f* than the sample containing alumina (sample R-100-20). We recall the results for polyamide-6

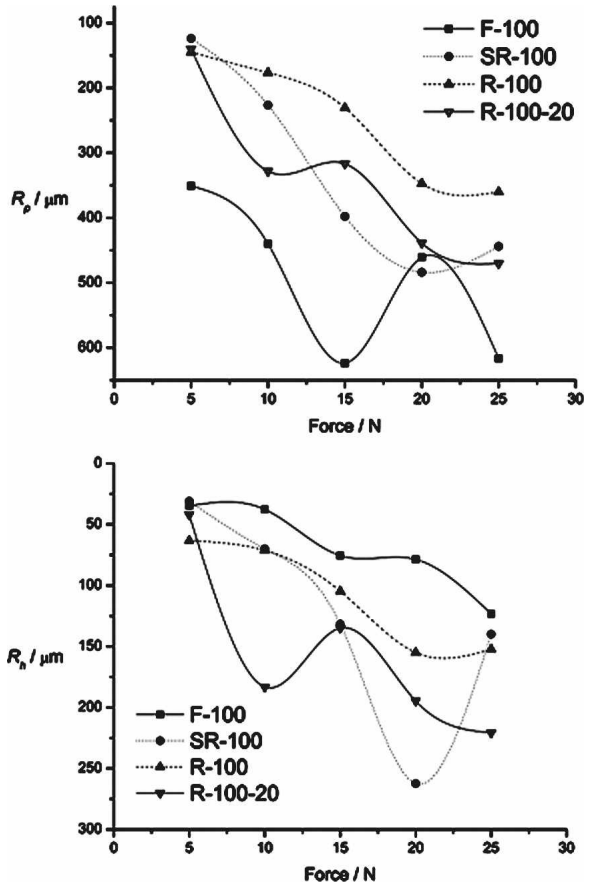

FIG. 5. R_p and R_h during single scratches plotted versus the force applied.

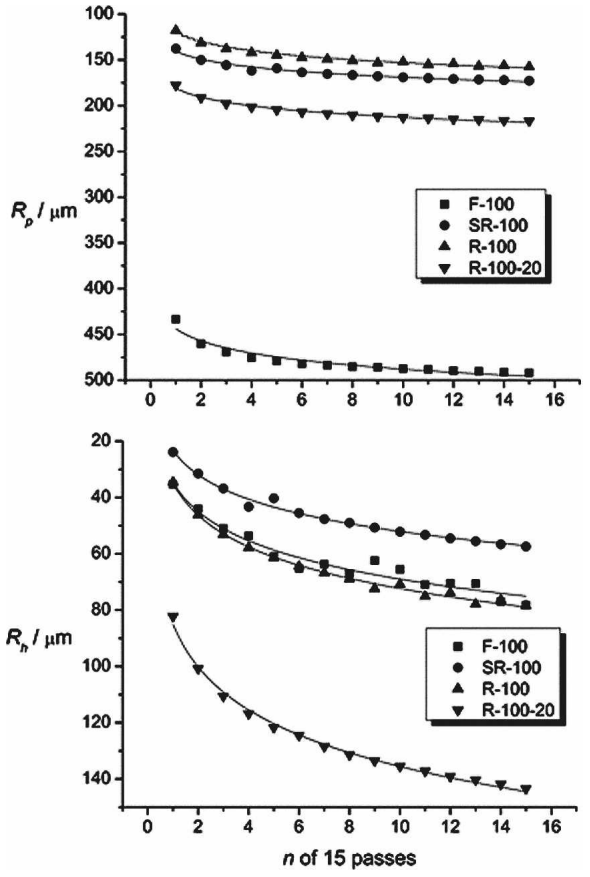

FIG. 6. R_p and R_h from sliding wear for each pass of the indenter.

reinforced with multiwalled carbon nanotubes (CNTs); CNTs provide mechanical strengthening but hamper the *f*.[57] The semi-rigid material exhibits intermediate values, although it tends more toward rigid behavior than flexible.

In tests of sliding wear, we evaluate the behavior of the obturation materials during repetitive scratching. The depths are plotted as a function of the number of passes of the indenter: after about 10 passes, the beginning of a plateau is observed in the R_p values (Fig. 6); however, values of R_h appear to continue to worsen. Generally, the observance of strain hardening in polymer-based materials (PBMs) is defined by the asymptotic behavior of both R_p and R_h curves.[50,52] For our materials, the behavior observed here suggests that repetitive wear does not significantly increase penetration but damages the material such that it recovers less with each pass of the indenter.

Overall, the R_p was highest for the F-100 sample (Figs. 5 and 6), while for sliding wear under a 5 N applied load the R-100 sample has the most shallow R_p. Values for the semi-rigid and rigid samples without alumina are somewhat higher. This is similar to the cluster of values at a load of 5 N seen above in Fig. 5 for R_p after single scratching. Most important is the *f* of the samples. Similar to the results for single scratches (at a load of 5 N), in sliding wear the SR-100 sample has the lowest R_h, while the F-100 and R-100 samples have slightly higher values and the R-100-20 sample has the highest value. Thus, the highest concentration of alumina we used hampered the *f* the most. Note that even the highest recorded value of R_h for sample R-100-20 is approximately 140 μm, which is less than or equal to the pore diameters and the HAp particle sizes in all the samples.

D. Friction

The friction behavior of dental obturation materials is relevant in determining the durability of such materials. Figure 7 shows that friction is higher for the flexible and semi-rigid materials and as low as 0.4 for samples containing the rigid PU. Because we know that friction is related to other material properties, we are not surprised to find that the friction values support the results of the mechanical properties obtained and discussed earlier. We infer that the higher elastic modulus of the rigid materials plays a significant role in their lower friction.

V. A SURVEY OF RESULTS

New HAp-based hybrid porous materials were produced with morphology and mechanical properties appropriate for use as vascularized obturation materials.

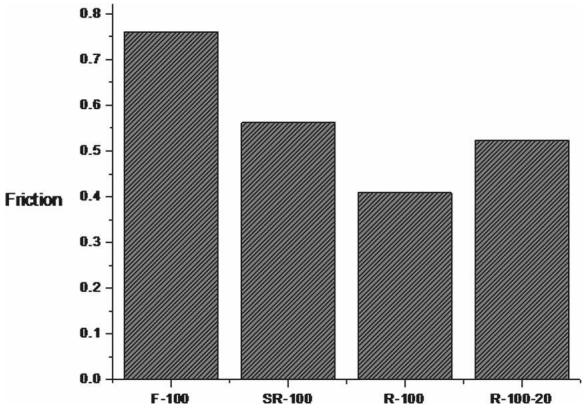

FIG. 7. Friction of the samples as determined by a pin-on-disk tribometer.

This represents a step forward in the design of dental materials because existing obturation materials are designed to be inert implants, while our materials are designed to actively encourage tooth attachment and regeneration. Our new biomaterials have interconnected pores with average pore size between 100 and 250 μm, and pore volume fractions ranging from 26% to 60%, thus making them viable candidates to simulate real teeth. The pore size and volume can be modified by changing the particle size of the HAp powder and the relative concentration of HAp/resin. This occurs because CO_2 formation depends on the availability of reactive groups; in turn, that availability depends on the resin/CA ratio; the amount of resin needed is dependent on the HAp particle size. As we establish a quantitative relationship between these components and the resultant morphology, we will improve our ability to predict and control the exact morphology of our materials.

While the flexible resin sample F-100 exhibits the best abrasion resistance and viscoelastic recovery f after scratching, and also possesses a pore size and volume fraction near the desired range, its weak mechanical properties discourage its use as a dental obturation filling. The semi-rigid sample SR-100 does not match the mechanical properties of the rigid materials and also exhibits poor resistance to abrasion, thereby negating its usefulness for the intended application.

The samples with the best performance are R-100, R-100-20, and R-100-40. Because their pore size is around 150 μm, the R-100 and R-100-40 samples possess the right morphology; a pore volume fraction near 50% should result in sufficient interconnection for vascular growth. The mechanical properties of the R-100 and R-100-40 samples are combined with a high abrasion resistance (5.5 and 4.7 × 10^{-5} g/s, respectively). Low friction along with good resistance to scratching, and decent f after single scratches and sliding wear suggest the usefulness of the rigid hybrids for obturation materials in dentistry. Given the wide range of rigidity available in PUs and our capability to vary concentrations of HAp and alumina, fine tuning of the desired properties is possible.

Finally, we note the issue of the sources of HAp. In this work, we have used a synthetic HAp. We recall that HAp can also be made from egg shells,[58] which otherwise become an environmental problem.

ACKNOWLEDGMENTS

The authors are in debt to Mrs. Alicia del Real for her valuable help in SEM analysis and to Mrs. Maribel Presa for the determination of the mechanical properties. Financial support to H.E.H. Lobland has been provided by a National Defense Science and Engineering Graduate (NDSEG) Fellowship (Washington, DC).

REFERENCES

1. D. Stojanovic, B. Jokic, Dj. Veljovic, R. Petrovic, P.S. Uskokovic, and Dj. Janackovic: Bioactive glass-apatite composite coating for titanium implant synthesized by electrophoretic deposition. *J. Eur. Ceram. Soc.* **27,** 1595 (2007).
2. C. Balázsi, F. Wéber, Z. Kövér, E. Horváth, and C. Németh: Preparation of calcium-phosphate bioceramics from natural resources. *J. Eur. Ceram. Soc.* **27,** 1601 (2007).
3. J.M. Anderson and J.J. Langone: Issues and perspectives on the biocompatibility and immunotoxicity evaluation of implanted controlled release systems. *J. Control. Release* **57,** 107 (1999).
4. M. Tanahashi, T. Yao, T. Kokubo, M. Minoda, T. Miyamoto, T. Nakamura, and T. Yamamuro: Apatite coated on organic polymers by biomimetic process improvement in its adhesion to substrate by NaOH treatment. *J. Appl. Biomater.* **5,** 339 (1994).
5. P.N. de Aza, F. Guitián, and S. de Aza: A new bioactive material which transforms in situ into hydroxyapatite. *Acta Mater.* **46,** 2541 (1998).
6. Y. Shikinami and M. Okuno: Bioresorbable devices made of forged composites of hydroxyapatite (HA) particles and poly-L-lactide (PLLA): Part I. Basic characteristics. *Biomaterials* **20,** 859 (1999).
7. M.E. Thomas, P.W. Richter, T. van Deventer, J. Crooks, and U. Ripamonti: Macroporous synthetic hydroxyapatite bioceramics for bone substitute applications. *S. Afr. J. Sci.* **95,** 359 (1999).
8. R. Schilke, J.A. Lisson, O. Baub, and W. Geurtsen: Comparison of the number and diameter of dentinal tubules in human and bovine dentine by scanning electron microscopic investigation. *Arch. Oral Biol.* **45**(5), 355 (2000).
9. R.S. Manly, H.C. Hodge, and L.E. Ange: Density and refractive index studies of dental hard tissues: II. Density distribution curves. *J. Dent. Res.* **15**, 203 (1939).
10. S.A. Patterson: In vivo and in vitro studies of the effect of disodium salt of ethylenediamine tetra-acetate on human dentine and its endodontic implications. *Oral Surg.* **16**(1), 83 (1987).
11. D.H. Pashley: Dentin-predentin complex and its permeability: Physiology overview. *J. Dent. Res.* **64,** 613 (1985).
12. L.B. Goldman, M. Goldman, J.H. Kronman, and P.S. Lin: The efficacy of several irrigations solutions for endodontics: A scanning electron microscopy study. *Oral Surg.* **52**(2), 197 (1985).

13. A. Cosijns, C. Vervaet, J. Luyten, S. Mullens, F. Siepmann, L. Van Hoorebeke, B. Masschaele, V. Cnudde, and J.P. Remon: Porous hydroxyapatite tablets as carriers for low-dosed drugs. *Eur. J. Pharmacol. Biopharmacol.* **67**(2), 498 (2007).
14. D. Gupta, S. Chandra, and S. Chandra: Effect of the smeared layer upon dentinal tubule penetration by root canal sealers: A SEM study. *Endodontology* **8**(1), 26 (1996).
15. S. Teng, L. Chen, Y. Guo, and J. Shi: Formation of nano-hydroxyapatite in gelatin droplets and the resulting porous composite microspheres. *J. Inorg. Biochem.* **101,** 686 (2007).
16. J.F. Piecuch: Long-term evaluation of the use of coralline hydroxyapatite in orthognathic surgery. *J. Oral Maxillofac. Surg.* **56,** 941 (1998).
17. N. Ozgür Engin and A. Cüney Tas: Manufacture of macroporous calcium hydroxyapatite bioceramics. *J. Eur. Ceram. Soc.* **19,** 2569 (1999).
18. L.K.A. Rodriguez, M.N. dos Santos, D. Pereira, A.V. Assaf, and V. Pardi: Carbon dioxide laser in dental caries prevention. *J. Dent.* **32,** 531 (2004).
19. H.J. Lee, S.E. Kim, H.W. Choi, C.W. Kim, K.J. Kim, and S.C. Lee: The effect of surface-modified nano-hydroxyapatite on biocompatibility of poly (E-caprolactone)/hydroxyapatite nanocomposites. *Eur. Polym. J.* **43,** 1602 (2007).
20. P.S. Uskokovic, C.Y. Tang, C.P. Tsui, N. Ignjatovic, and D.P. Uskokovic: Micromechanical properties of a hydroxyapatite/poly-L-lactide biocomposite using nanoindentation and modulus mapping. *J. Eur. Ceram. Soc.* **27,** 1559 (2007).
21. J.P. Paul: Strength requirements for internal and external prostheses. *J. Biomech.* **32,** 381 (1999).
22. M. Spector: Historical review of porous-coated implants. *J. Arthroplasty* **2,** 163 (1987).
23. P.H.F. Caria, E.Y. Kawachi, C.A. Bertran, and J.A. Camilli: Biological assessment of porous-implant hydroxyapatite combines with periosteal grafting in maxillary defects. *J. Oral Maxillofac. Surg.* **65,** 847 (2007).
24. M. Rabello: *Putting Additives into Polymers* (Artliber, Sao Paulo 2000), Chap. 10.
25. L.H. He and M.V. Swain: Enamel: A "metallic-like" deformable biocomposite. *J. Dent.* **35,** 431 (2007).
26. C-L. Lin, S-H. Chang, J-C. Wang, and W-J. Chang: Mechanical interactions of an implant/tooth-supported system under different periodontal supports and number of splinted teeth with rigid and non-rigid connections. *J. Dent.* **34,** 682 (2006).
27. B. Fischman: The rotational aspect of mandibular flexure. *J. Prosth. Dent.* **64,** 483 (1990).
28. A. de la Isla, W. Brostow, B. Bujard, M. Estevez, J.R. Rodriguez, S. Vargas, and V.M. Castaño: Nanohybrid scratch resistant coatings for teeth and bone viscoelasticity manifested in tribology. *Mater. Res. Innovat.* **7**(2), 110 (2003).
29. M. Estevez, S. Vargas, H.E. Hagg Lobland, A. de la Isla, W. Brostow, and J. Rogelio Rodrıguez: Characterization of novel dental obturation materials. *Mater. Res. Innovat.* **10**(4), 411 (2006).
30. V.M. Castaño and R. Rodriguez: Polymer-based hybrid organic-inorganic materials, in *Performance of Plastics,* edited by W. Brostow (Hanser, Munich, 2000), Chap. 24.
31. M. Deng and S.W. Shalaby: Polymers as biomaterials, in *Performance of Plastics,* edited by W. Brostow (Hanser, Munich, 2000), Chap. 23.
32. C. Hengtrakool, G.J. Pearson, and M. Wilson: Interaction between GIC and S Sanguis biofilms: Antibacterial properties and changes of surfaces hardness. *J. Dent.* **34,** 588 (2006).
33. T.J. Griffin and W.S. Cheung: The use of short, wide implants in posterior areas with reduced bone height: A retrospective investigation. *J. Prosth. Dent.* **92,** 139 (2004).
34. J.W. Freudenthaler, G.K. Tischler, and C.J. Burstone: Bond strength of fiber-reinforced composite bars for orthodontic attachment. *Am. J. Orthod. Dentofacial Orthop.* **120,** 648 (2001).
35. F. Tancret, J-M. Bouler, J. Chamousset, and L-M. Minois: Modelling the mechanical properties of microporous and macroporous biphasic calcium phosphate bioceramics. *J. Eur. Ceram. Soc.* **26,** 3647 (2006).
36. C.E. Aragon and R.N. Bohay: The application of alveolar distraction osteogenesis following nonresorbable hydroxyapatite grafting in the anterior maxilla: A clinical report. *J. Prosth. Dent.* **93,** 518 (2005).
37. R.P. Wool: Interfaces and adhesion, in *Performance of Plastics,* edited by W. Brostow (Hanser, Munich, 2000), Chap. 15.
38. R. Mülhaupt: Toughened thermoplastics and thermosets, in *Performance of Plastics*, edited by W. Brostow (Hanser, Munich, 2000), Chap. 20.
39. Z. Roslaniec, G. Broza, and K. Schulte: Nanocomposites based on multiblock polyester elastomers (PEEs) and carbon nanotubes (CNTs). *Compos. Interfaces* **10,** 95 (2003).
40. A. Bismarck, M. Hofmeier, and G. Dörner: Effect of hot water immersion on the performance of carbon reinforced unidirectional poly(ether ether ketone) (PEEK) composites: Stress rupture under end-loaded bending. *Composites A* **38,** 407 (2007).
41. A. Kopczynska and G.W. Ehrenstein: Polymeric surfaces and their true surface tension in solids and melts. *J. Mater. Ed.* **29,** 325 (2007).
42. W. Brostow, J.V. Duffy, G.F. Lee, and K. Madejczyk: Parameters of equation of state of polyurethanes from acoustic resonance and isobaric expansivity. *Macromolecules* **24,** 479 (1991).
43. E.B. Mano: *Polymers as Engineering Materials* (Edgard Blücher, São Paulo, 1996).
44. L.G. Griffith: Polymeric biomaterials. *Acta Mater.* **48,** 263 (2000).
45. W. Brostow, B. Bujard, P.E. Cassidy, H.E. Hagg, and P.E. Montemartini: Effects of fluoropolymer addition to an epoxy on scratch depth and recovery. *Mater. Res. Innovat.* **6,** 7 (2001).
46. W. Brostow, J-L. Deborde, M. Jaklewicz, and P. Olszynski: Tribology with emphasis on polymers: Friction, scratch resistance and wear. *J. Mater. Ed.* **25,** 119 (2003).
47. W. Brostow and M. Jaklewicz: Tribology of a polymeric molecular composite: Effects of magnetic field orientation. *J. Mater. Res.* **19,** 1038 (2004).
48. M. Estevez, S. Vargas, V.M. Castaño, J.R. Rodriguez, H.E. Hagg Lobland, and W. Brostow: Novel wear resistant and low toxicity dental obturation materials. *Mater. Lett.* **61,** 3025 (2007).
49. W. Brostow, W. Chonkaew, L. Rapoport, Y. Soifer, and A. Verdyan: Grooves in microscratch testing. *J. Mater. Res.* **22,** 2483 (2007).
50. W. Brostow, G. Damarla, J. Howe, and D. Pietkiewicz: Determination of wear of surfaces by scratch testing. *e-Polymers* **025,** 1 (2004).
51. M.D. Bermudez, W. Brostow, F.J. Carrion-Vilches, J.J. Cervantes, and D. Pietkiewicz: Wear of thermoplastics determined by multiple scratching. *e-Polymers* **005,** 1 (2005).
52. W. Brostow, H.E. Hagg Lobland, and M. Narkis: Sliding wear, viscoelasticicity, and brittleness of polymers. *J. Mater. Res.* **21,** 2422 (2006).
53. L. Vujosevic and K. Obradovic-Durici: Porosity of hard dental tissues. *Stomatol. Glasnik Serb.* **36**(2), 95 (1989).

54. W. Brostow, A.M. Cunha, J. Quintanilla, and R. Simões: Predicting cracking phenomena in molecular dynamics simulations of polymer liquid crystals. *Macromol. Theory Simul.* **11,** 308 (2002).
55. W. Brostow and R. Simões: Tribological and mechanical behavior of polymers simulated by molecular dynamics. *J. Mater. Ed.* **27,** 19 (2005).
56. E. Rivera-Muñoz, R. Velázquez, and R. Rodríguez: Improvement in mechanical properties of hydroxyapatite objects with controlled porosity made by modified gelcasting process. *Mater. Sci. Forum* **426–432,** 4489 (2003); on line at http://www.scientific.net.
57. L.F. Giraldo, W. Brostow, E. Devaux, B.L. Lopez, and L.D. Perez: Scratch and wear resistance of polyamide 6 reinforced with multiwall carbon nanotubes. *J. Nanosci. Nanotechnol.* **8,** (2008, in press).
58. E.M. Rivera, M. Araiza, W. Brostow, V.M. Castaño, J.R. Diaz-Estrada, R. Hernández, and J.R. Rodríguez: Synthesis of hydroxyapatite from eggshells. *Mater. Lett.* **41,** 128 (1999).